

Granular Calcium Carbonate Reinforced the Cement Paste Cured by Elevated Temperatures

Yanming Li* and Kaiqiang Liu*

Cite This: *ACS Omega* 2023, 8, 8346–8354

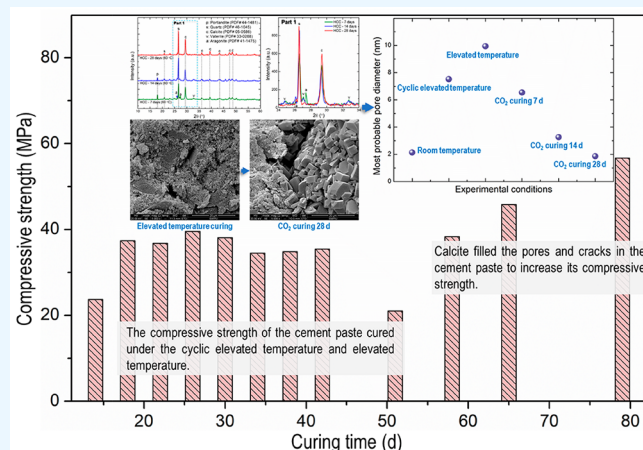
Read Online

ACCESS |

Metrics & More

Article Recommendations

ABSTRACT: In a heavy oil thermal recovery well, cement paste experiences the cyclic elevated temperature and steam of steam stimulation, the elevated temperature and steam of steam driving, and the high-concentration CO₂ (HCC) of in situ combustion conditions in sequence. To understand the effects of different conditions of heavy oil thermal recovery wells on the properties and microstructure of the cement paste, this paper investigated the influence of the cyclic elevated temperature, elevated temperature, and high-concentration CO₂ conditions on the compressive strength of the cement paste. Then, low-field nuclear magnetic resonance, scanning electron microscopy, and X-ray diffraction were used to test the pore structure, microstructure, and crystal type of the cement paste cured under different conditions. Experimental results showed that the elevated temperature curing loosened the microstructure of the cement paste and increased its pore size and porosity, resulting in reducing the compressive strength to 21.04 MPa, compared with that of the cement paste at cyclic elevated temperature. For the cement paste cured under high-concentration CO₂ conditions, the calcium hydroxide and calcium-silicate-hydrate reacted with CO₂ to generate granular vaterite, aragonite, and calcite in the pores and cracks, which repaired the cement paste by reducing the porosity and pore size of the cement paste and increasing its compressive strength. When the carbonation time increased to 28 days, the cement paste was completely carbonized, and the compressive strength of the cement paste increased by approximately 169%, compared with that of the cement paste cured at an elevated temperature.



1. INTRODUCTION

In petroleum engineering, cement-based materials have been used to isolate the stratum and protect the metal casing.^{1–3} However, the complex conditions of oil and natural gas wells, i.e., high temperatures and pressures, among other factors, can strongly affect the structural integrity and mechanical properties of the cement paste.^{4–10} Particularly, In the heavy oil thermal recovery process, cement paste usually experiences the cyclic elevated temperature and steam (CETS) of steam stimulation (SS), the elevated temperature and steam (ETS) of steam driving (SD), and the high-concentration CO₂ (HCC) of in situ combustion conditions in sequence.¹¹ Researchers generally believe that understanding the effects of the CETS, ETS, and HCC conditions of heavy oil thermal recovery on the microstructure and properties of the cement paste is very important for designing the cement slurry of heavy oil cementing and ensuring the integrity of the cement sheath.^{4,12,13}

In the exploitation of heavy oil, the SS technique increases the reservoir temperature and reduces the viscosity of the heavy oil by injecting steam with an elevated temperature of 300–320 °C repeatedly into the heavy oil reservoir.^{11,14–16} During this

process, the wellbore containing the cement paste is repeatedly heated and cooled.^{17–20} The SD technique continuously injects steam at elevated temperatures (approximately 350 °C) into the heavy oil reservoir^{21–24} to increase the recovery efficiency of heavy oil. In situ combustion injects air into the heavy oil reservoir through the injection well to make the heavy oil self-ignite and heat the reservoir, which can also improve the recovery efficiency of heavy oil. Figure 1 shows a diagram of the in situ combustion operation. During the in situ combustion, the temperature of the firing line was over 500 °C, and a large amount of CO₂ was emitted. However, the firing line moved slowly; before it reached the cement sheath, the temperature of the cement sheath was low¹⁶ (this study set the temperature as

Received: November 3, 2022

Accepted: February 14, 2023

Published: February 24, 2023



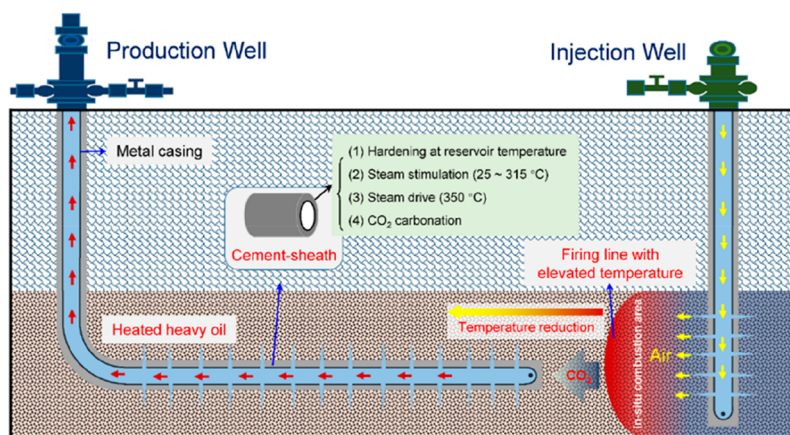


Figure 1. Environment of the cement sheath of a heavy oil production well during in situ combustion.

Table 1. Chemical Composition of G-Class Cement and Metakaolin

sample	density (g/cm ³)	composition (wt %)								
		CaO	SiO ₂	Al ₂ O ₃	Fe ₂ O ₃	MgO	K ₂ O	TiO ₂	SO ₃	LOI
G cement	3.15	62.91	21.40	2.76	5.14	1.16	0.81	0.28	0.82	4.72
metakaolin	2.6		42.01	36.46	0.88	0.83		0.39		19.43
quartz	2.45	0.83	97.93	0.14	0.86	0.05	0.03		0.10	0.06

60 °C²⁵), but CO₂ might have a significant impact on cement sheath.

Currently, there are some publications on the effect of elevated temperature on the microstructure and properties of Portland cement paste. For example, Piasta et al.^{26–28} reported that a high-temperature environment would destroy the microstructure of calcium silicate hydrates (C–S–H), worsening the mechanical properties and pore structure of the cement paste. Alonso et al.²⁸ found that, at an elevated temperature of 200 °C, some chain- or netlike C–S–H changed to nesosilicate, but when the curing temperature was increased to 450 °C, all the C–S–H changed to nesosilicate, which destroyed the mechanical properties of the cement paste. However, there are a few publications on the effect of CETS and ETS conditions on the chemical structure, microstructure, and properties of cement paste. Additionally, it has been reported in the literature^{29–33} that when cement paste was exposed to a high concentration of CO₂, CO₂, or CO₃²⁻ diffused into the cracks and pores of the cement paste, Ca(OH)₂ and C–S–H were carbonized to form both crystalline and amorphous calcium carbonate.^{34–37} Because the volume of CaCO₃ is larger than that of the original Ca(OH)₂ in the cement paste, the growth of CaCO₃ increases the internal stress of the cement paste, producing cracks and reducing the mechanical properties of the cement paste.^{38–40} However, in these publications, the cement pastes did not experience curing under the CETS and ETS conditions. It is thus difficult to explain the carbonation behavior and mechanism of the cement paste after CETS and ETS curing in the heavy oil thermal recovery process.^{17,34,41}

In this study, to fully understand the influence of the heavy oil thermal recovery process on the properties and microstructure of cement paste, first, an elevated temperature and steam curing device¹⁷ and high-temperature carbonation device³⁴ were developed to investigate the effects of CETS, ETS, and HCC conditions on the compressive strength of the cement paste. Second, the pore structure of the cement paste cured under different conditions was tested using low-field nuclear magnetic

resonance (LFNMR). By combination of phenolphthalein titration^{36,42} and X-ray diffraction (XRD) methods, the carbonation rate and crystal phase of the cement paste after CETS and ETS curing were studied. Finally, a scanning electron microscope (SEM) was utilized to observe the micromorphology of the carbonation products and to study the effect of CO₂ carbonation on the microstructure of the cement paste after CETS and ETS curing. These experimental achievements can further enrich our understanding of the carbonation behavior and mechanism of the cement-based materials and provide new insights for designing and optimizing the cement system for the cementing operation of heavy oil wells.

2. EXPERIMENTAL MATERIALS AND METHODS

2.1. Materials. In this study, high-sulfate-resistance G-class oil well cement (G cement), produced according to the API-10A standard,⁴³ was provided by Xinjiang Tianshan Cement Co., Ltd. Quartz and metakaolin were used to control the high-temperature resistance of the cement paste. The stability and rheological properties of the cement slurry were controlled by fluid-loss additives and dispersants, to meet the requirements for cement slurry properties in cementing engineering of a heavy oil well.⁴⁴ The chemical compositions of G cement, metakaolin, and quartz were tested using X-ray fluorescence. Before sample testing, all samples were dried at 105 °C for 2 h, and the loss on ignition (LOI) was recorded. Table 1 shows the chemical composition of the G cement, quartz, and metakaolin. In this experiment, the cement paste consisted of G cement, 25 wt % quartz, 10 wt % metakaolin, 2 wt % fluid-loss additive, 0.8 wt % dispersant, and 54 wt % water. This cement formulation has been used in the cementing operation of heavy oil wells by the Xinjiang Oilfield Company.

2.2. Methods. **2.2.1. Curing Method.** Heavy oil thermal recovery includes steam stimulation, steam driving, and in situ combustion. To accurately simulate the service environments of the cement paste in steam stimulation and steam driving, we developed a new CETS curing device (Figure 2). Detailed

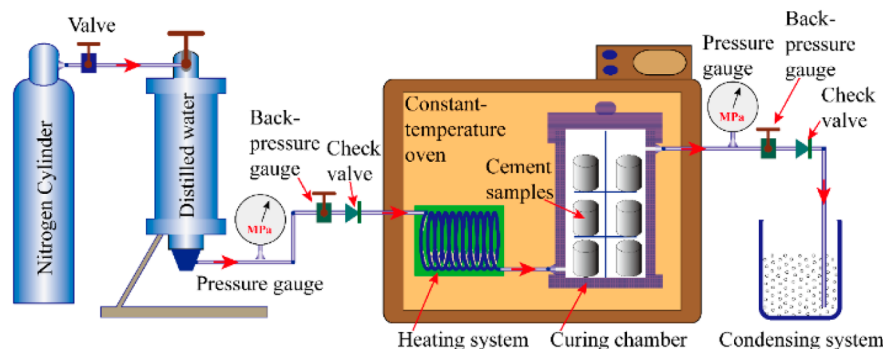


Figure 2. Diagram of cyclic elevated temperature and the steam curing device. Reprinted with permission from ref 17. Copyright 2020 Elsevier.

information on the device was reported in a previous work.¹⁷ The nitrogen cylinder provided steady pressure to inject distilled water into the curing chamber with CETS or ETS. The curing pressure of the curing chamber is controlled by a check valve, and the constant temperature oven provided the cyclic elevated temperature condition.

According to the data for a heavy oil well from the Xinjiang Oilfield Company,¹⁵ when the steam stimulation is implemented, the highest temperature is 315 °C, whereas the temperature of steam driving is approximately 350 °C. Therefore, by combining the data and laboratory conditions, we designed the experimental temperature, as shown in Figure 3.

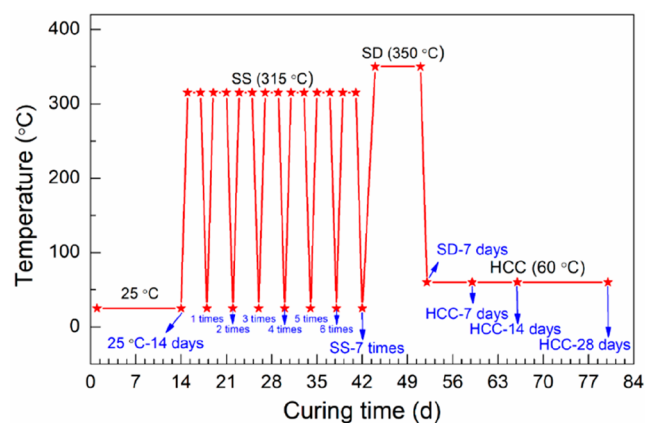


Figure 3. Curing temperatures under different conditions.

The preparation of the cement samples and the curing procedure were as follows: The cement paste samples with a cylinder mold (diameter, 25.4 mm; height, 25.4 mm) were prepared and cured for 14 days at 25 °C. Then the samples were put into the CETS curing device to continuously simulate the SS-7 times¹⁷ and SD-7 days (350 °C).^{45,46}

After the samples experienced CETS and ETS curing, the samples were put into a high-temperature and high-pressure container in the CO₂ corrosion experiment. Then, gas with a partial pressure of CO₂ of 2 MPa, partial pressure of N₂ of 8 MPa, and total pressure of 10 MPa⁴⁷ was injected into the container. The temperature of the container was set as 60 °C.²⁵ The corrosion times of the cement paste were 7, 14, and 28 days. During each curing stage of the cement paste, some cement samples were taken out to test the compressive strength, phase, microstructure, and pore structure.

2.2.2. Compressive Strength Test. According to the experimental conditions shown in Figure 3, the cement paste

continuously experienced 25 °C curing for 14 days, CETS curing 7 times (28 days), ETS curing for 7 days, and CO₂ carbonation for 28 days. Under the different curing conditions, once the curing temperature decreased to 25 or 60 °C, the cement samples were taken out. The compressive strength of the cement paste was tested with a loading rate of 72 ± 7 kN/min.

2.2.3. XRD and Microstructure Analysis. X-ray diffraction (DX-2700X, Haoyuan Instrument) with a scanning rate of 0.02°/s was used to test the XRD patterns of the cement paste cured at 25 °C for 14 days (RT-14 days) and then subjected to CETS curing 7 times (SS-7 times), ETS curing for 7 days (SD-7 days), CO₂ carbonation for 7 days (HCC-7 days), CO₂ carbonation for 14 days (HCC-14 days), and CO₂ carbonation for 28 days (HCC-28 days). The XRD patterns of the cement paste ranged from 10° to 60°. Additionally, an environmental scanning electron microscope (ESEM) (Quanta 450, FEI Company) was utilized to observe the microstructure of the cement samples.

2.2.4. Pore Structure Test. These cement samples cured under different conditions were treated by vacuum-saturated water. Then the Carr–Purcell–Meiboom–Gill method and LFNMR (MicroMR, Niumag Instrument Corporation) were utilized to analyze the pore structure of these cement samples cured under CETS, ETS, and HCC conditions, by testing the transverse relaxation time (T_2) of hydrogen protons in the pores of cement samples.^{1,48,49} The relation between T_2 and pore size of the cement paste is expressed as

$$\frac{1}{T_2} \approx \gamma \frac{2}{R} \quad (1)$$

where γ is the relaxivity. Zhou et al.⁵⁰ reported that the relaxivity of the cement paste is 1.88 nm/ms. R is the pore radius in the cement paste.^{51,52}

Through the further calculation of LFNMR data, the porosity, ϕ_{NMR} , can be obtained using

$$\phi_{\text{nmr}} = \sum_i \frac{m_i S_b G_b V_B}{M_b s g \vartheta} \times 100\% \quad (2)$$

where m_i is the T_2 increment, M_b is the total T_2 amplitude of the standard sample, S_b is the scanning time of the standard sample, s is the scanning time of the cement paste, G_b is the receiver gain of the standard sample, g is the receiver gain of the cement paste, V_b is the total water volume of the standard sample, and ϑ is the volume of the cement paste.

3. RESULTS

3.1. Compressive Strength. Figure 4 presents the compressive strength of the cement pastes cured under 25 °C,

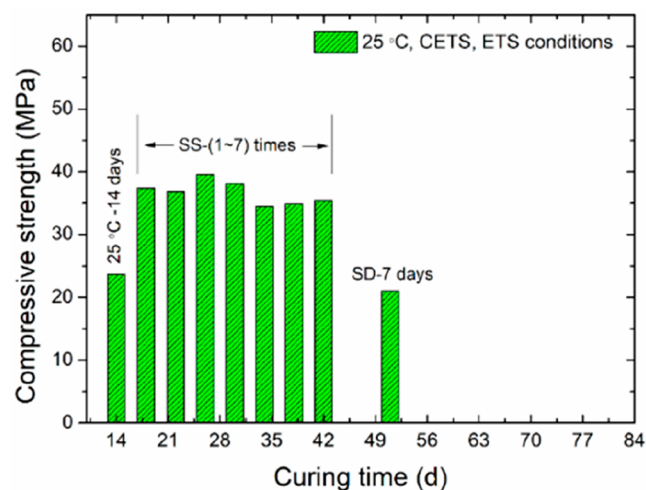


Figure 4. Compressive strength of the cement paste cured under CETS and ETS conditions.

CETS, and ETS conditions. From the results of Figure 4, it can be seen that when the curing time was 14 days at 25 °C, the compressive strength of the cement paste reached 23.7 MPa. Its compressive strength cured at CETS (the highest temperature is 315 °C) for 1 time increased to 37.41 MPa. With increasing CETS curing time, the compressive strength of the cement paste did not change significantly, and when the CETS curing increased 7 times, the compressive strength of the cement paste was 35.46 MPa. Previous works have indicated that cement paste cured for 14 days at 25 °C is difficult to hydrate completely. Under CETS conditions, the hydration degree of the cement paste increased with increasing hydration time. However, when the ETS curing reached 7 days, its compressive strength rapidly decreased from 35.46 to 21.04 MPa.

In situ combustion of heavy oil emits significant amounts of CO₂ that carbonizes the cement paste (see Figure 1).^{30,40} Figure 5 shows the compressive strength of the cement paste carbonized for 7, 14, and 28 days under HCC conditions. It can be seen that, with increasing carbonation time, the compressive strength obviously increased. At HCC-7 days, the compressive strength of the cement paste increased from 21.04 to 38.34 MPa, increasing by 82.22%. At HCC-28 days, its compressive strength was 56.65 MPa, increasing by 169% compared to that of the cement paste cured at SD-7 days. The increase in compressive strength of the cement paste in the current study is thus obviously higher than that of the published results.⁵³

3.2. CO₂ Corrosion Rate. The carbonation rate of the cement paste cured for different times under HCC conditions was analyzed using the phenolphthalein titration experiment.³⁶ In this experiment, first, the cross sections of the cement paste carbonized for different times under HCC conditions were obtained. Next, the phenolphthalein solution was titrated to the cross sections. The carbonation of the cement paste causes a reaction among Ca(OH)₂, C–S–H, and CO₂, reducing the pH value of the carbonation area. When the alkaline hydration products meet the phenolphthalein solution, the color of the hydration products changes to red. Therefore, through

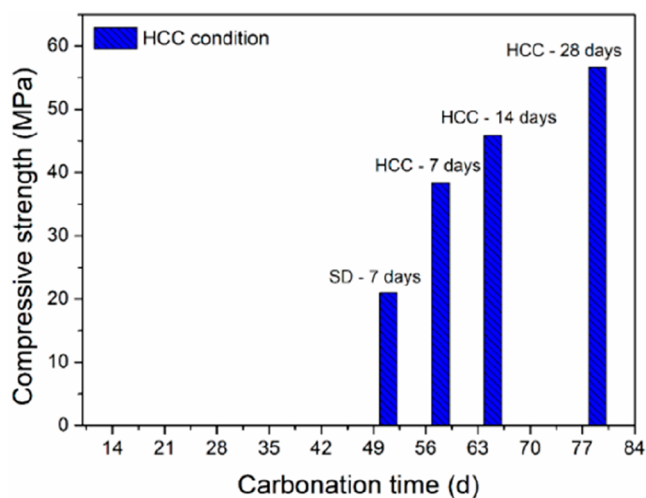


Figure 5. Compressive strength of the cement paste carbonized under HCC conditions.

observing the color of the cross sections, the carbonation rate and degree of the cement paste cured under HCC conditions can be obtained.³⁴

Figure 6 presents the results of the phenolphthalein titration of the cement paste carbonized for different times under HCC

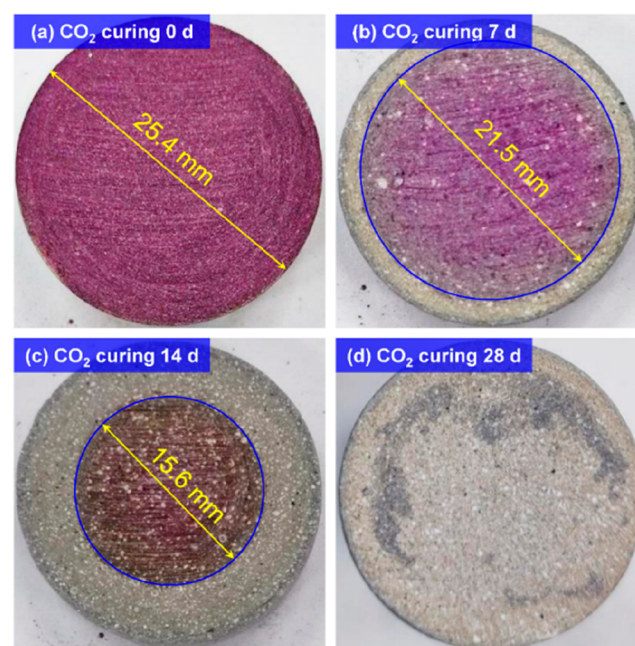


Figure 6. Phenolphthalein titration photos of the cement paste carbonized for different times under HCC conditions: (a) CO₂ curing 0 days; (b) CO₂ curing 7 days; (c) CO₂ curing 14 days; (d) CO₂ curing 28 days.

conditions. From the results of Figure 6, it can be seen that when the carbonation time of the cement paste increased to 28 days, the red area in the cement paste could not be observed, which indicated that the cement paste was almost completely carbonized. Compared to the results of Gu et al.,³⁴ after the cement paste experienced CETS and ETS curing, the carbonation rate of the cement paste increased significantly.

3.3. Pore Structure Analysis. Figure 7 shows the transverse relaxation time (T_2) of the cement paste cured under different

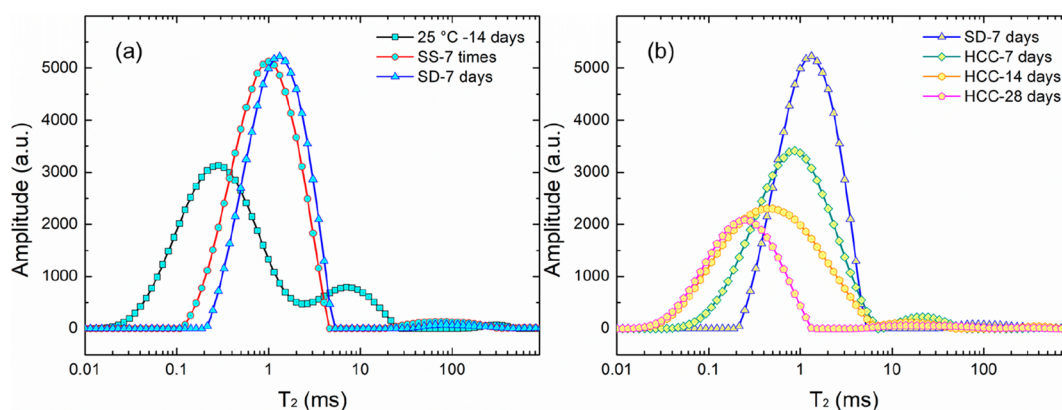


Figure 7. T_2 results of the cement paste cured under (a) CETS and ETS and (b) HCC conditions.

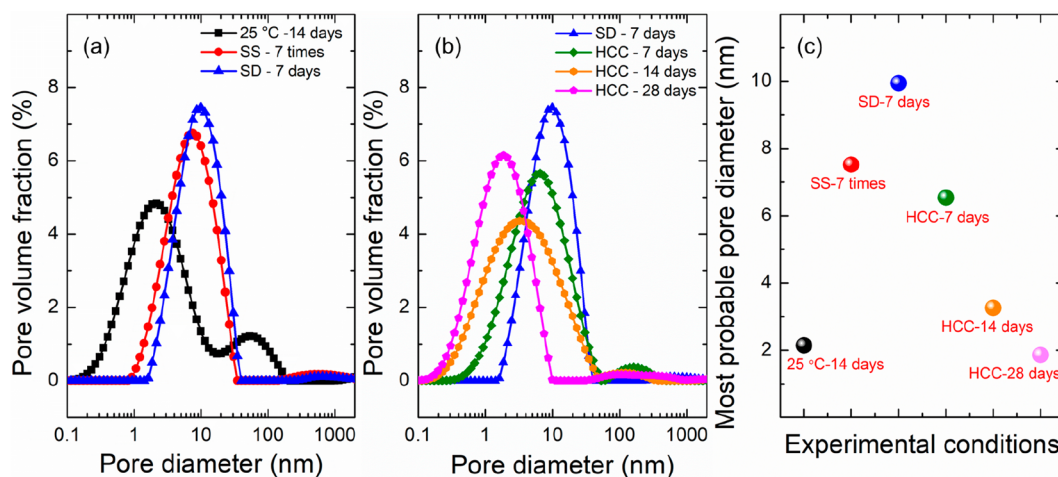


Figure 8. Pore-size of the cement paste cured under (a) CETS and ETS and (b) HCC conditions. (c) Most probable pore diameter.

conditions. The T_2 of the cement paste moves to the right with increasing CETS and ETS curing time. When the cement paste enters the CO_2 corrosion process, the T_2 of the cement paste moves to the left with increasing the corrosion time. Based on eq 3, T_2 and the pore size of the cement paste have a linear relation. Therefore, the results of Figure 7 further illustrate that different curing conditions change the pore structure of the cement paste.

Based on the results of Zhou et al.,⁵⁰ the relaxivity of the cement paste is 1.88 nm/ms. Combining the T_2 of the cement paste and the relaxivity, the pore size of the cement paste cured under different conditions could be calculated using eq 1. Figure 8 shows the pore-size distribution and the most probable diameter of the cement paste. The pore size of the cement paste cured for 14 days at 25 °C was 0.4–180 nm, and the most probable diameter was 2.14 nm. The pore size can be divided into two peaks at 10 nm. Muller et al.⁵⁴ reported that the pore size of the cement paste less than 10 nm is related to C–S–H. The pore size larger than 50 nm corresponds to the capillary pores in the cement paste.

When the CETS curing time increased to 7 times, the pore size of the cement paste ranged from 0.9 to 30 nm, and the most probable pore diameter was 7.52 nm. When the cement paste experienced ETS curing for 7 days, its pore size ranged from 1.6 to 34 nm, and the most probable pore diameter was 9.94 nm. Therefore, CETS and ETS curing increased the pore size of the cement paste and changed the microstructure of C–S–H in the cement paste.

The porosity of the cement paste can be calculated on the basis of the T_2 results of the cement paste and eq 2. Table 2

Table 2. Porosity of the Cement Paste Cured at Different Conditions

conditions	25 °C, 14 days	SS-7 times	SD-7 days	HCC-7 days	HCC-14 days	HCC-28 days
porosity (%)	21.03	28.75	29.47	22.82	20.75	18.04

presents the porosity of the cement paste. From the results of Table 2, it can be seen that the porosity of the cement paste after CETS and ETS curing increased significantly. However, the porosity of the cement paste decreased with increasing CO_2 carbonation time.

3.4. XRD. Figure 9 shows the XRD patterns of the cement paste cured under the 25 °C, CETS, and ETS conditions. The main crystal phases in the cement paste include $\text{Ca}(\text{OH})_2$ [powder diffraction file (PDF) 44-1481], SiO_2 (PDF 46-1045), and C–S–H (PDF 33-0306). The diffraction peaks at 18.06°, 28.73°, and 34.16° are related to $\text{Ca}(\text{OH})_2$, and the diffraction peaks at 20.88°, 26.68°, and 36.59° are related to quartz (SiO_2). The diffraction peaks of C–S–H include 29.38° and 32.12°. Compared to the cement paste cured at 25 °C, curing with CETS and ETS conditions did not change the crystal phases of the cement paste. The cement paste cured under ETS conditions and the intensity of the $\text{Ca}(\text{OH})_2$ diffraction peaks

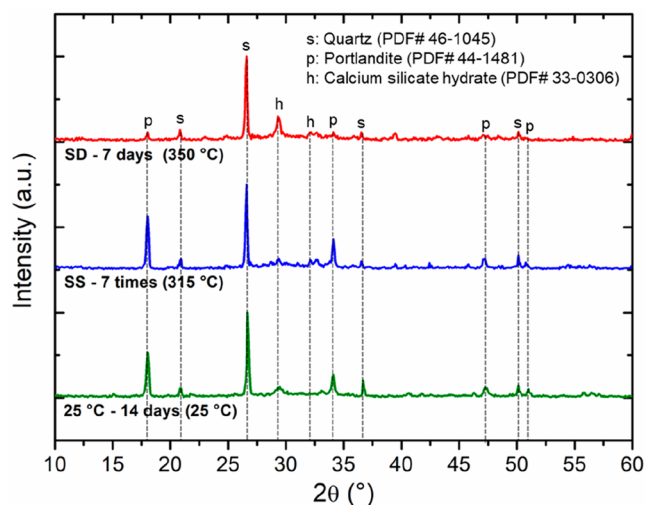


Figure 9. XRD patterns of the cement paste cured under CETS and ETS conditions.

decreased significantly with increasing curing time. The main reason for the peak intensity decrease of the cement paste may be that $\text{Ca}(\text{OH})_2$ and SiO_2 had a pozzolanic reaction to consume the $\text{Ca}(\text{OH})_2$ at elevated temperatures and steam conditions.

After the cement paste experienced CETS and ETS curing, it was cured under HCC conditions. Figure 10 shows the XRD patterns of the cement paste cured for different times under HCC conditions. In the figure, c, a, and v are calcite, aragonite, and vaterite, respectively. The diffraction peaks of calcite (PDF 05-0586) include 29.4° , 36.0° , 39.4° , 43.2° , 47.5° , and 48.5° ; the diffraction peaks at 26.2° and 27.2° are related to the aragonite (PDF 41-1475), and the diffraction peaks at 24.9° , 27.0° , and 32.8° are associated with the vaterite (PDF 33-0268). It can thus be seen that when the cement paste was cured for 7 days under HCC conditions, the crystal phases in the cement paste included aragonite, vaterite, calcite, and SiO_2 . Compared to the results of Figure 10, when the cement paste cured for 7 days under HCC conditions, some $\text{Ca}(\text{OH})_2$ of the cement paste reacted with CO_2 to form CaCO_3 , and some C–S–H reacted with CO_2 to generate CaCO_3 and silica gel.¹² When the cement paste was

carbonized for 14 days under HCC conditions, the diffraction peaks of aragonite almost disappeared. With increasing carbonation time, when the cement paste was carbonized for 28 days under HCC conditions, the diffraction peak of vaterite and aragonite almost disappeared; its main crystal phases include SiO_2 and calcite.

3.5. Microstructure Analysis. Figure 11 shows the SEM images of the cement paste cured at 25°C -14 days, SS-7 times, SD-7 days, CC-7 days, HCC-14 days, and HCC-28 days. A comparative analysis of Figure 11a–c shows that after the cement paste was cured at SS-7 times, the microstructure of some hydration products showed an increase in the pore size of those hydration products.

When the cement paste was continuously cured at SD-7 days, the hydration products in the cement paste loosened, resulting in an obvious increase in the pore size and porosity of the cement paste. Figure 11d–f presents the SEM images of the cement paste corroded at CC-7 days, CC-14 days, and CC-28 days, respectively. When the cement paste was carbonized for 7 days, some carbonation products filled the cracks and pores, increasing the density of the cement paste. Based on the XRD results, the particles' carbonation products were aragonite, vaterite, and calcite. With increasing carbonation time, the particle carbonation products grew, and some phases changed to calcite. Because the C–S–H in the cement paste reacted with CO_2 to generate CaCO_3 and silica gel⁵⁵ at the same time, amorphous silica gel can be observed in Figure 11f.

Combining the results of Figures 11 and 12, with increasing CO_2 carbonation time, vaterite, aragonite, and calcite filled the cracks and pores of the cement paste. Compared with lamellar $\text{Ca}(\text{OH})_2$, CaCO_3 has better mechanical properties. CaCO_3 fills the cracks and pores, which can improve the compressive strength of the cement paste.

4. GENERAL DISCUSSION

Combining the results of Figures 9 and 10, the phases of the cement paste cured under the CETS conditions did not exhibit obvious changes. Previous work¹⁷ has reported that cement paste cured for 14 days at 25°C contained some unhydrated cement. A high curing temperature accelerated the hydration of the cement paste and improved the pozzolanic reaction between hydration products and metakaolin and SiO_2 to increase the

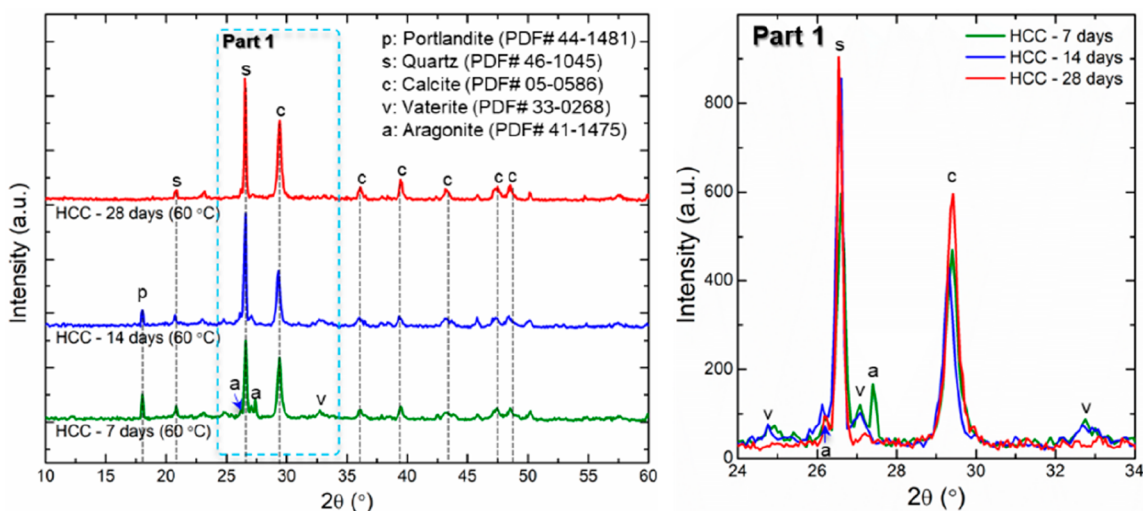


Figure 10. XRD patterns of the cement paste cured under HCC conditions.

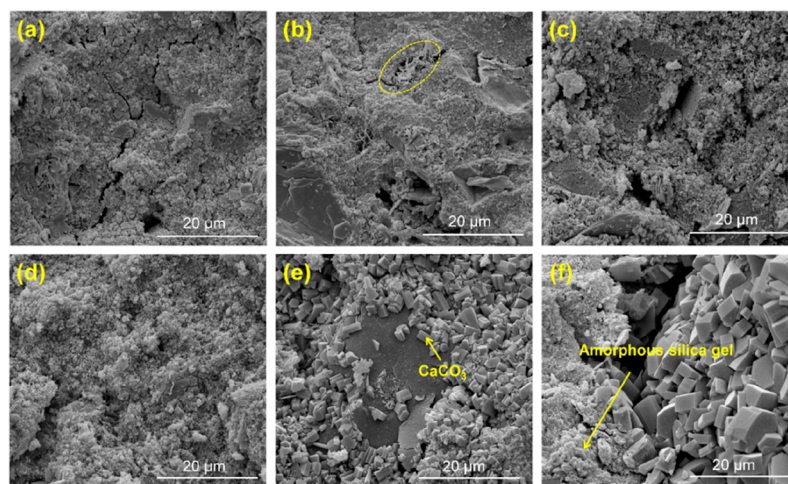


Figure 11. Microstructure of cement paste cured at (a) 25 °C-14 days; (b) SS-7 times; (c) SD-7 days; (d) HCC-7 days; (e) HCC-14 days; and (f) HCC-28 days.

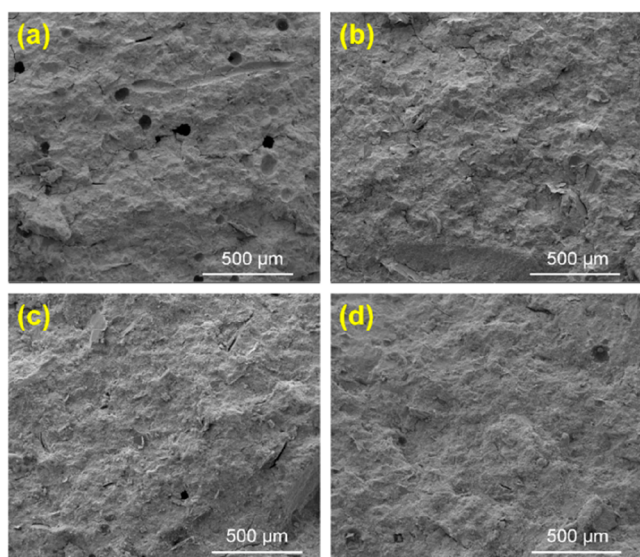


Figure 12. Microstructure of cement paste cured for different times under CO₂ conditions: (a) SD-7 days; (b) HCC-7 days; (c) HCC-14 days; and (d) HCC-28 days.

content of the hydration products in the cement paste and to improve the compressive strength of the cement paste. When the cement paste experienced ETS curing, the silicon chain of C-S-H and the microstructure of the cement paste were destroyed, thus increasing the pore size and porosity of the cement paste, as shown in Figure 13. The compressive strength results show that, for the cement paste cured for 7 days under ETS conditions, its strength decreased by 40.67% compared with that of CETS curing conditions cured for 7 times.

Then the cement paste continuously cured under HCC conditions. Compared with the results of Gu et al.,^{34,42} the carbonation rate and compressive strength of the cement paste cured by CETS and ETS conditions rapidly increased during the CO₂ carbonation process. When the carbonation time reached 28 days, the compressive strength of the cement paste increased by 169% to 56.65 MPa. Based on published results^{53,56} in the cement paste, C-S-H and Ca(OH)₂ reacted with CO₂ to form CaCO₃ (as shown in eqs 3 and 4), repairing the cracks and pores of the cement paste produced by CETS and ETS curing. With

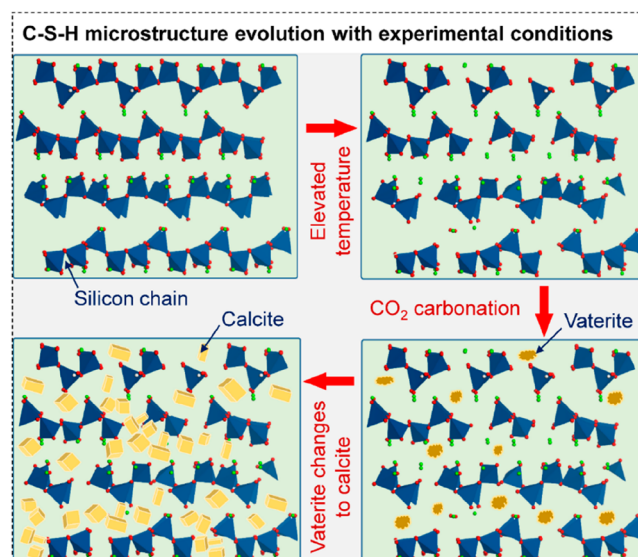
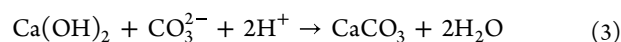


Figure 13. Effects of ETS and CO₂ carbonation conditions on the microstructure of C-S-H.

increasing carbonation time, the CaCO₃ crystals grew, thus decreasing the pore size and porosity of the cement paste. Moreover, the mechanical properties of lamellar Ca(OH)₂ are lower than those of CaCO₃. Figure 13 shows the microstructure evolution of C-S-H cured at ultrahigh temperature and the repair process of CO₂ on the cement paste after CETS and ETS curing. Therefore, the carbonization of the cement paste formed CaCO₃, thus decreasing the porosity and pore size, which is the main reason for the improved compressive strength of the cement paste. Additionally, ETS curing increased the pore size of the cement paste to improve the diffusion and migration rate of CO₂ in the cement paste, which accelerated the carbonization rate of the cement paste.



5. CONCLUSIONS

Based on the experimental results and the discussion, we can draw the following conclusions:

- (1) Comparing the effects of CETS and ETS curing conditions on the compressive strength of the cement paste, the CETS conditions did not have an obvious influence on the compressive strength of the cement paste. However, ETS curing rapidly decreased the compressive strength of the cement paste. When ETS curing time reached 7 days, its compressive strength decreased from 35.46 to 21.04 MPa.
- (2) According to the XRD results of the cement paste cured under CETS and ETS conditions, CETS and ETS curing did not change the crystal phases of the cement paste. Combining its SEM microstructure illustrated that the curing conditions led its microstructure to loosen, and increased its porosity and pore size.
- (3) The porosity and pore size of the cement paste after CETS and ETS curing increased, which improved the diffusion and migration rate of CO₂ in the cement paste and accelerated the carbonation rate. In the HCC condition, Ca(OH)₂ and C–S–H reacted with CO₂ to generate a large amount of CaCO₃ in the cracks and pores. Then, the growth of CaCO₃ decreased the pore size and porosity of the cement paste and improved its mechanical properties. When the carbonation time reached 28 days, the compressive strength of the cement paste increased by 169%.

This research provides a new ideal for designing and optimizing cement systems in the cementing operation of heavy oil, and the achievements provide new insight for understanding the CO₂ carbonation of cement-based materials.

AUTHOR INFORMATION

Corresponding Authors

Yanming Li – China Coal Technology Engineering Group (CCTEG) Chongqing Research Institute, Chongqing 400039, China; Email: lngdlym@126.com

Kaiqiang Liu – School of New Energy and Materials, Southwest Petroleum University, Chengdu 610500, China; orcid.org/0000-0002-8866-026X; Email: kaiqiangliu@swpu.edu.cn

Complete contact information is available at:
<https://pubs.acs.org/10.1021/acsomega.2c07090>

Notes

The authors declare no competing financial interest.

ACKNOWLEDGMENTS

The authors appreciate the financial support provided by National Natural Science Foundation of China (No. 52104007) and State Key Laboratory of Gas Disaster Monitoring and Emergency Technology (No. 2021SKLKF08). We really appreciate the experimental assistance provided by the State Key Laboratory of Oil & Gas Reservoir Geology and Exploitation.

REFERENCES

(1) Liu, K.; Yang, X.; Zhang, H.; Yao, S.; Huang, Z.; Zhang, X.; Cao, Q.; Li, B.; Luo, Z.; Cheng, X.; Yang, Z.; Chi, C. Pore connectivity of oil well cement in the early hydration stage by in situ electrical resistivity measurements and low-field nuclear magnetic resonance, *Constr. Build. Mater.* **2021**, *303*, 124448.

(2) Liu, K.; Yang, Y.; Zhang, X.; Zhu, K.; Wang, J.; Li, L.; Tu, Q.; Ma, R.; Cheng, X.; Zhang, X. Time-varying characteristics and mechanisms of hydrostatic pressure descent of Portland cement slurry. *Powder Technol.* **2021**, *385*, 434–443.

(3) Munjal, P.; Hau, K. K.; Hon Arthur, C. C. Effect of GGBS and curing conditions on strength and microstructure properties of oil well cement slurry. *J. Build. Eng.* **2021**, *40*, 102331.

(4) Kutchko, B. G.; Strazisar, B. R.; Dzombak, D. A.; Lowry, G. V.; Thaulow, N. Degradation of well cement by CO₂ under geologic sequestration conditions, *Environ. Sci. Technol.* **2007**, *41*, 4787–4792.

(5) Barlet-Gouédard, V.; Rimmelé, G.; Porcherie, O.; Quisel, N.; Desroches, J. A solution against well cement degradation under CO₂ geological storage environment. *Int. J. Greenh. Gas Control.* **2009**, *3*, 206–216.

(6) Bachu, S. CO₂ storage in geological media: Role, means, status and barriers to deployment. *Prog. Energy Combust. Sci.* **2008**, *34*, 254–273.

(7) Carey, J. W. Geochemistry of wellbore integrity in CO₂ sequestration: Portland cement-steel-brine-CO₂ interactions. *Rev. Mineral. Geochemistry.* **2013**, *77*, 505–539.

(8) Liu, K.; Cheng, X.; Ma, Y.; Gao, X.; Zhang, C.; Li, Z.; Zhuang, J. Analysis of interfacial nanostructure and interaction mechanisms between cellulose fibres and calcium silicate hydrates using experimental and molecular dynamics simulation data. *Appl. Surf. Sci.* **2020**, *506*, 144914.

(9) Liu, K.; Cheng, X.; Zhang, X.; Guo, X.; Zhuang, J. Design of low-density cement optimized by cellulose-based fibre for oil and natural gas wells. *Powder Technol.* **2018**, *338*, 506–518.

(10) Cheng, X.; Liu, K.; Zhang, X.; Li, Z.; Guo, X. Integrity changes of cement sheath due to contamination by drilling fluid. *Adv. Cem. Res.* **2018**, *30*, 47–55.

(11) Yuan, S.; Jiang, H.; Shi, Y.; Ren, Z.; Wang, J.; Zhang, Y. Study on heavy oil components transformation path based on core analysis during in-situ combustion process. *Fuel.* **2019**, *253*, 72–78.

(12) Liaudat, J.; Martínez, A.; López, C. M.; Carol, I. Modelling acid attack of oilwell cement exposed to carbonated brine. *Int. J. Greenh. Gas Control.* **2018**, *68*, 191–202.

(13) Abid, K.; Gholami, R.; Choate, P.; Nagaratnam, B. H. A review on cement degradation under CO₂-rich environment of sequestration projects. *J. Nat. Gas Sci. Eng.* **2015**, *27*, 1149–1157.

(14) Yuan, S.; Jiang, H.; Ren, Z.; Wang, H.; Zhang, Y.; Bai, Y. A new description method of the position of combustion front in dry linear fire flooding process. *Int. Commun. Heat Mass Transfer* **2020**, *113*, 104530.

(15) Xi, C.; Guan, W.; Jiang, Y.; Liang, J.; Zhou, Y.; Wu, J.; Wang, X.; Cheng, H.; Huang, J.; Wang, B. Numerical simulation of fire flooding for heavy oil reservoirs after steam injection: A case study on Block H1 of Xinjiang Oilfield, NW China. *Pet. Explor. Dev.* **2013**, *40*, 766–773.

(16) Guan, W.; Xi, C.; Chen, Y.; Zhang, X.; Muhetar, Liang, J.; Huang, J.; Wu, J. Fire-flooding technologies in post-steam-injected heavy oil reservoirs. *Pet. Explor. Dev.* **2011**, *38*, 452–463.

(17) Zhang, X.; Yang, J.; Li, K.; Pu, H.; Meng, X.; Zhang, H.; Liu, K. Effects of steam on the compressive strength and microstructure of cement paste cured under alternating ultrahigh temperature. *Cem. Concr. Compos.* **2020**, *112*, 103681.

(18) Wang, X.; Wang, J.; Qiao, M. Horizontal well, nitrogen and viscosity reducer assisted steam huff and puff technology: Taking super heavy oil in shallow and thin beds, Chunfeng Oilfield, Junggar Basin, NW China, as an example. *Pet. Explor. Dev.* **2013**, *40*, 104–110.

(19) Xu, A.; Mu, L.; Fan, Z.; Wu, X.; Zhao, L.; Bo, B.; Xu, T. Mechanism of heavy oil recovery by cyclic superheated steam stimulation. *J. Pet. Sci. Eng.* **2013**, *111*, 197–207.

(20) Xianghong, W.; Anzhu, X.; Hailiang, F. An integrated evaluation on factors affecting the performance of superheated steam huff and puff in heavy oil reservoirs. *Pet. Explor. Dev.* **2010**, *37*, 608–613.

(21) Cao, Y.; Liu, D.; Zhang, Z.; Wang, S.; Wang, Q.; Xia, D. Steam channeling control in the steam flooding of super heavy oil reservoirs, Shengli Oilfield. *Pet. Explor. Dev.* **2012**, *39*, 785–790.

(22) Huang, S.; Chen, X.; Liu, H.; Xia, Y.; Jiang, J.; Cao, M.; Li, A.; Yang, M. Experimental and numerical study of steam-chamber

evolution during solvent-enhanced steam flooding in thin heavy-oil reservoirs. *J. Pet. Sci. Eng.* **2019**, *172*, 776–786.

(23) Huang, S.; Chen, X.; Liu, H.; Jiang, J.; Cao, M.; Xia, Y. Experimental and numerical study of solvent optimization during horizontal-well solvent-enhanced steam flooding in thin heavy-oil reservoirs. *Fuel* **2018**, *228*, 379–389.

(24) Lyu, X.; Liu, H.; Pang, Z.; Sun, Z. Visualized study of thermochemistry assisted steam flooding to improve oil recovery in heavy oil reservoir with glass micromodels. *Fuel* **2018**, *218*, 118–126.

(25) Yuan, S.; Jiang, H.; Yang, F.; Shi, Y.; Bai, Y.; Du, K. Research on characteristics of fire flooding zones based on core analysis. *J. Pet. Sci. Eng.* **2018**, *170*, 607–610.

(26) Piasta, J.; Sawicz, Z.; Rudzinski, L. Changes in the structure of hardened cement paste due to high temperature. *Matériaux Constr.* **1984**, *17*, 291–296.

(27) Krakowiak, K. J.; Thomas, J. J.; Musso, S.; James, S.; Akono, A. T.; Ulm, F. J. Nano-chemo-mechanical signature of conventional oil-well cement systems: Effects of elevated temperature and curing time. *Cem. Concr. Res.* **2015**, *67*, 103–121.

(28) Alonso, C.; Fernandez, L. Dehydration and rehydration processes of cement paste exposed to high temperature environments. *J. Mater. Sci.* **2004**, *39*, 3015–3024.

(29) Bachu, S.; Bennion, D. B. Experimental assessment of brine and/or CO₂ leakage through well cements at reservoir conditions. *Int. J. Greenh. Gas Control.* **2009**, *3*, 494–501.

(30) Bihua, X.; Bin, Y.; Yongqing, W. Anti-corrosion cement for sour gas (H₂S-CO₂) storage and production of HTHP deep wells. *Appl. Geochem.* **2018**, *96*, 155–163.

(31) Conde Silva, J.; Milestone, N. B. Cement/rock interaction in geothermal wells. The effect of silica addition to the cement and the impact of CO₂ enriched brine. *Geothermics.* **2018**, *73*, 16–31.

(32) Chen, T.; Gao, X. How carbonation curing influences ca leaching of Portland cement paste: Mechanism and mathematical modeling. *J. Am. Ceram. Soc.* **2019**, *102*, 7755–7767.

(33) Zajac, M.; Skibsted, J.; Ben Haha, M. Effect of alkalis on enforced carbonation of cement paste: Mechanism of reaction. *J. Am. Ceram. Soc.* **2021**, *104*, 1076–1087.

(34) Gu, T.; Guo, X.; Li, Z.; Cheng, X.; Fan, X.; Korayem, A.; Duan, W. H. Coupled effect of CO₂ attack and tensile stress on well cement under CO₂ storage conditions. *Constr. Build. Mater.* **2017**, *130*, 92–102.

(35) Wang, D.; Noguchi, T.; Nozaki, T.; Higo, Y. Investigation of the carbonation performance of cement-based materials under high temperatures. *Constr. Build. Mater.* **2021**, *272*, 121634.

(36) Rita Damasceno Costa, A.; Pereira Gonçalves, J. Accelerated carbonation of ternary cements containing waste materials. *Constr. Build. Mater.* **2021**, *302*, 124159.

(37) Park, S.; Moon, H.; Kim, J. H.; Lee, M.; Chung, C. W. Reaction of hydrated cement paste with supercritical carbon dioxide. *Constr. Build. Mater.* **2021**, *281*, 122615.

(38) De Ceukelaire, L.; Van Nieuwenburg, D. Accelerated carbonation of a blast-furnace cement concrete. *Cem. Concr. Res.* **1993**, *23*, 442–452.

(39) Ishihara, K.; Funahashi, M.; Hanaki, N.; Miyata, M.; Yamamoto, H. Influence of porosity and water content on the diffusivity of CO₂ and O₂ through hydrated cement paste. *Synlett.* **1994**, *24*, 963–964.

(40) Bagheri, M.; Shariatipour, S. M.; Ganjian, E. A review of oil well cement alteration in CO₂-rich environments. *Constr. Build. Mater.* **2018**, *186*, 946–968.

(41) Yang, Y.; Yuan, B.; Wang, Y.; Zhang, S.; Zhu, L. Carbonation resistance cement for CO₂ storage and injection wells. *J. Pet. Sci. Eng.* **2016**, *146*, 883–889.

(42) de Sena Costa, B. L.; de Oliveira Freitas, J. C.; Silva Santos, P. H.; Gomes da Silva Araújo, R.; dos Santos Oliveira, J. F.; de Araújo Melo, D. M. Study of carbonation in a class G Portland cement matrix at supercritical and saturated environments. *Constr. Build. Mater.* **2018**, *180*, 308–319.

(43) American Petroleum Institute (API). *API 10A: Specification for cements and materials for well cementing*; API, 2002.

(44) American Petroleum Institute (API). *API 10B-2: Recommended practice for testing well cements*; API, 2013.

(45) Guo, K.; Li, H.; Yu, Z. In-situ heavy and extra-heavy oil recovery: A review. *Fuel* **2016**, *185*, 886–902.

(46) Kayukova, G. P.; Mikhailova, A. N.; Kosachev, I. P.; Nasyrova, Z. R.; Gareev, B. I.; Vakhin, A. V. Catalytic Hydrothermal Conversion of Heavy Oil in the Porous Media. *Energy and Fuels.* **2021**, *35*, 1297–1307.

(47) Neuville, N.; Aouad, G.; Lecolier, E.; Damidot, D. Innovative leaching tests of an oilwell cement paste for CO₂ storage: Effect of the pressure at 80°C. *Energy Procedia.* **2012**, *23*, 472–479.

(48) Bhattacharja, S.; Moukwa, M.; D’Orazio, F.; Jehng, J. Y.; Halperin, W. P. Microstructure determination of cement pastes by NMR and conventional techniques. *Adv. Cem. Based Mater.* **1993**, *1*, 67–76.

(49) Zhou, C.; Ren, F.; Zeng, Q.; Xiao, L.; Wang, W. Pore-size resolved water vapor adsorption kinetics of white cement mortars as viewed from proton NMR relaxation. *Cem. Concr. Res.* **2018**, *105*, 31–43.

(50) Zhou, C.; Ren, F.; Zeng, Q.; Xiao, L.; Wang, W. Pore-size resolved water vapor adsorption kinetics of white cement mortars as viewed from proton NMR relaxation. *Cem. Concr. Res.* **2018**, *105*, 31–43.

(51) Liu, K.; Cheng, X.; Li, J.; Gao, X.; Cao, Y.; Guo, X.; Zhuang, J.; Zhang, C. Effects of microstructure and pore water on electrical conductivity of cement slurry during early hydration. *Compos. Part B Eng.* **2019**, *177*, 107435.

(52) Liu, K.; Cheng, X.; Zhang, C.; Gao, X.; Zhuang, J.; Guo, X. Evolution of pore structure of oil well cement slurry in suspension-solid transition stage. *Constr. Build. Mater.* **2019**, *214*, 382–398.

(53) Ashraf, W. Carbonation of cement-based materials: Challenges and opportunities. *Constr. Build. Mater.* **2016**, *120*, 558–570.

(54) Muller, A. C. A.; Scrivener, K. L. A reassessment of mercury intrusion porosimetry by comparison with ¹H NMR relaxometry. *Cem. Concr. Res.* **2017**, *100*, 350–360.

(55) Ashraf, W. Carbonation of cement-based materials: Challenges and opportunities. *Constr. Build. Mater.* **2016**, *120*, 558–570.

(56) Morandau, A.; Thiéry, M.; Dangla, P. Investigation of the carbonation mechanism of CH and C-S-H in terms of kinetics, microstructure changes and moisture properties. *Cem. Concr. Res.* **2014**, *56*, 153–170.